Mode Matching in Microstrip Antenna with both Electric and Magnetic Surface Current on Sidewall in Cavity Model

Fazel Rangriz Rostami, Gholamreza Moradi, and Reza Sarraf Shirazi

Department of Electrical Engineering
Amirkabir University of Technology, Tehran, Iran
fazel.rangriz@aut.ac.ir, ghmoradi@aut.ac.ir, sarraf@aut.ac.ir

Abstract ─ A model is developed to calculate the input impedance of a coaxially fed circular microstrip disc antenna in L band and C band. A mode matching approach with both electric and magnetic surface current is used, which makes it possible to improve the effects of modes. In addition, the method of images is used to remove the ground plane. Finally comparison is made with CST studio results, as it can be seen the theoretical calculations for input impedance are in good agreement with CST studio results except for minor shift in frequency.

Index Terms ─ Antennas, cavity model, input impedance, microstrip antennas, mode matching,

I. INTRODUCTION

Some papers have studied the subject of input impedance for microstrip antennas of various configurations [1], [2]. Several papers analyze coaxial feed microstrip antenna in conjunction with the cavity model of circular disk with different techniques, e.g., Green's function technique [3], Vector Hankel Transform with Galerkin's method [4], equivalent current ribbon mode [5], and multiport analysis [6]. An improved cavity model formulation to predict accurate input impedance of coax-fed circular microstrip antenna has been reported in [7]. Computation and optimization of input impedance of coax-fed microstrip antenna are discussed in [8].

The present paper uses cavity Green's-function technique along with mode matching technique for evaluating the input impedance of a probe-fed circular ring microstrip antenna. Figure 1 shows the antenna, which consists of a circular disk mounted on a grounded dielectric, the antenna has a radius equal to a, the fringing fields along the circumference of the antenna are taken into account by replacing the patch radius a by the effective radius a_e [9]. Antenna is driven by a coaxial line through the ground plane at radial distance r_0 from the center of the patch. The thickness and the dielectric constant of the substrate are denoted by h and ε, respectively. In order to have less frequency shift compared with CST studio results, effective dielectric constant can be used [9]. The permeability μ of the substrate is equal to that of the air, i.e., $\mu = \mu_0$. To determine the input impedance of the antenna, it is necessary to find the electric field solution beneath the circular patch [10]. In general this solution takes the form of a cylindrical mode expansion, with each mode being determined to within an arbitrary constant. To find all of these constants additional boundary conditions are required, which are obtained by considering the wall admittances. These wall admittances y_n fix the ratio between the z – directed electric field and the ϕ – directed magnetic field for each mode [10]. In this paper we use both electric and magnetic surface currents on the sidewall in cavity model in order to calculate the sidewall admittance. It is noticeable that, considering both currents do not appear to be available in the literature.

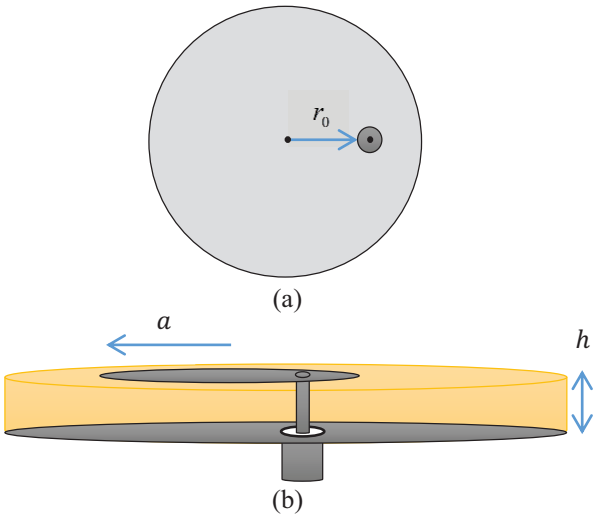

Fig. 1. Geometry of microstrip disc antenna: (a) top view of patch, and (b) 3D structure.

Submitted On: November 17, 2015
Accepted On: February 26, 2016

II. CALCULATION OF WALL ADMITTANCE

As shown in Fig. 2, region *I* is defined by $r < a$, and region *II* is defined by $r > a$, the method of images is used to remove the ground plane, so that the sidewall extends along the $z-$axis from $-h$ to $+h$.

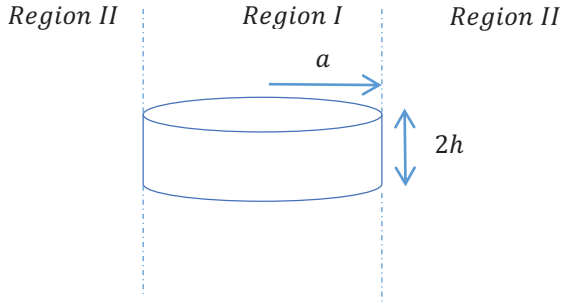

Fig. 2. Two regions of the problem.

In order to calculate wall admittance at the boundary between regions *I* and *II*, electric and magnetic fields with respect to the electric and magnetic vector potential in cylindrical coordinate are written as [12]:

$$E_\phi = \frac{\frac{\partial}{\partial r}F_z(r,\phi,z)}{\varepsilon_0} - \frac{\frac{\partial}{\partial z}\frac{\partial}{\partial \phi}A_z(r,\phi,z)i}{\omega r \varepsilon_0 \mu_0}, \quad (1)$$

$$E_z = -\omega A_z(r,\phi,z)i - \frac{\frac{\partial^2}{\partial z^2}A_z(r,\phi,z)i}{\omega \varepsilon_0 \mu_0}, \quad (2)$$

$$H_\phi = -\frac{\frac{\partial}{\partial r}A_z(r,\phi,z)}{\mu_0} - \frac{\frac{\partial}{\partial z}\frac{\partial}{\partial \phi}F_z(r,\phi,z)i}{\omega r \varepsilon_0 \mu_0}, \quad (3)$$

$$H_z = -\omega F_z(r,\phi,z)i - \frac{\frac{\partial^2}{\partial z^2}F_z(r,\phi,z)i}{\omega \varepsilon_0 \mu_0}, \quad (4)$$

where i is imaginary unit. Applying Fourier transform and Fourier series with respect to z and ϕ variables, respectively, result in Helmholtz equation for z component of vector potentials:

$$\left(r^2\frac{\partial^2}{\partial r^2} + r\frac{\partial}{\partial r} + k_r{}^2 r^2 - n^2\right)\begin{Bmatrix}\tilde{A}_z(r,\phi)\\ \tilde{F}_z(r,\phi)\end{Bmatrix} = 0, \quad (5)$$

in which $k_r = \sqrt{k_0{}^2 - k_z{}^2}$, and k_0 is the free space wave number, in every region and $-\infty < k_z < \infty$, solution of Helmholtz equation leads to the following equations:

$$\tilde{A}_z^{\,I} = h_n e^{in\phi} J_n(k_r r), \quad (6)$$

$$\tilde{F}_z^{\,I} = q_n e^{in\phi} J_n(k_r r), \quad (7)$$

$$\tilde{A}_z^{\,II} = f_n e^{in\phi} H_n^{(2)}(k_r r), \quad (8)$$

$$\tilde{F}_z^{\,II} = g_n e^{in\phi} H_n^{(2)}(k_r r), \quad (9)$$

where J_n and $H_n^{(2)}$ are Bessel function of the first kind and Hankel function of the second kind, respectively. h_n, q_n, f_n and g_n are constant values. By substituting (6)-(9) in (1)-(4), electric and magnetic field in every region can be obtained.

The boundary conditions on surface of the wall are given by:

$$\tilde{H}^{II}_{\phi,n}(a,\phi) - \tilde{H}^{I}_{\phi,n}(a,\phi) = \tilde{J}_{z,n}, \quad (10)$$

$$\tilde{E}^{I}_{z,n}(a,\phi) - \tilde{E}^{II}_{z,n}(a,\phi) = -\tilde{M}_{\phi,n}, \quad (11)$$

$$\tilde{H}^{I}_{z,n}(a,\phi) = \tilde{H}^{II}_{z,n}(a,\phi), \quad (12)$$

$$\tilde{E}^{I}_{\phi,n}(a,\phi) = \tilde{E}^{II}_{\phi,n}(a,\phi). \quad (13)$$

Magnetic and electric surface current on wall surface in main space and in Fourier space is as following:

$$\vec{J}(\phi,z) = \hat{z}\sum_n J_n e^{in\phi}\{U(h+z) - U(z-h)\}$$

$$\vec{\tilde{J}}(\phi,k_z) = \hat{z}\sum_n J_n e^{in\phi}\frac{2\sin(hk_z)}{k_z}, \quad (14)$$

$$\vec{M}(\phi,z) = \hat{\phi}\sum_n M_n e^{in\phi}\{U(h+z) - U(z-h)\}$$

$$\vec{\tilde{M}}(\phi,k_z) = \hat{\phi}\sum_n M_n e^{in\phi}\frac{2\sin(hk_z)}{k_z}, \quad (15)$$

in which $U(z)$ is the unit step function. By substituting (14) and (15) in (10) and (11), respectively, h_n, q_n, f_n and g_n are found with respect to J_n and M_n, then inverse Fourier transform are applied. Because of inverse transform, each equation has $exp(i\,k_z z)$ term. In order to eliminate the z dependence of equations, averaging with respect to z variable is taken as following:

$$\frac{\int_{-h}^{h} e^{ik_z z}\,dz}{2h} = \frac{\sin(hk_z)}{hk_z}, \quad (16)$$

then, wall admittances y_n are defined as ratio between the $z-$directed electric field and the $\phi-$directed magnetic field for each mode in main space [10]:

$$H^{II}_{\phi,n}(a,\phi) = -y_n E^{II}_{z,n}(a,\phi), \quad (17)$$

$$H_\phi(a,\phi) = \sum_n J_n e^{in\phi}, \quad (18)$$

$$E_\phi(a,\phi) = \sum_n M_n e^{in\phi}, \quad (19)$$

$$J_n = -y_n M_n. \quad (20)$$

After some mathematical simplification, the following equation for y_n can be obtained:

$$y_n^1 = \frac{\frac{\left(C^2 - 2AD + C\sqrt{B^2 - 4AD + C^2 + 2BC} + BC\right)}{2A}}{C} + D, \quad (21)$$

$$y_n^2 = -\frac{\frac{\left(2AD - C^2 + C\sqrt{B^2 - 4AD + C^2 + 2BC} - BC\right)}{2A}}{C} - D, \quad (22)$$

in which, A, B, C and D have integral form as following:

$$A = \frac{1}{\pi}\int_0^{\infty} \frac{\sin^2(hk_z)}{hk_z} \frac{k_r{}^2 H_n^{(2)}(ak_r) J_n(ak_r)}{2\omega k_z \varepsilon_0} dk_z, \quad (23)$$

$$B = -\frac{1}{\pi}\int_0^{\infty} \frac{\sin^2(hk_z)}{hk_z} \left(\frac{\omega n \varepsilon_0 J_n(ak_r) H_n^{(2)}(ak_r) i}{2\omega a k_z \varepsilon_0} - \frac{\omega a k_r \varepsilon_0 J_{n+1}(ak_r) H_n^{(2)}(ak_r) i}{2\omega a k_z \varepsilon_0}\right) dk_z, \quad (24)$$

$$C = -\frac{1}{\pi}\int_0^{\infty} \frac{\sin^2(hk_z)}{hk_z} \frac{k_r H_n'^{(2)}(ak_r) J_n(ak_r) i}{2k_z} dk_z, \quad (25)$$

$$D = \frac{1}{\pi}\int_0^{\infty} \frac{\sin^2(hk_z)}{hk_z} \left(\frac{\omega \varepsilon_0 H_n'^{(2)}(ak_r) J_{n+1}(ak_r)}{2k_z} - \frac{nak_r \varepsilon_0 \mu_0 \omega H_n'^{(2)}(ak_r) J_n(ak_r)}{2a^2 k_r{}^2 k_z \mu_0} - \frac{n^2 k_z H_n^{(2)}(ak_r) J_n(ak_r)}{2\omega a^2 k_r{}^2 \mu_0}\right) dk_z. \quad (26)$$

Since the integrand is an even function of k_z, the lower limit of integrals is changed to zero and the integral values are doubled. Because the equation with respect to y_n is a second-order polynomial, it has two answers, for each mode we choose one that gives positive real part.

III. INPUT IMPEDANCE

For calculation of input impedance, electric field in microstrip antenna is given by [11]:

$$E_z(r_0) = I_0 \sum_{n=-\infty}^{\infty} \frac{\omega\mu_0 J_n(kr_0) Y_n(kr_0) i}{4} - \frac{\omega\mu_0 J^2{}_n(kr_0)\varsigma i}{4\xi}, \quad (27)$$

$$\varsigma = akY_{n+1}(ak)i + \omega a y_n \mu_0 Y_n(ak) - nY_n(ak)i,$$

$$\xi = ak J_{n+1}(ak)i + \omega a y_n \mu_0 J_n(ak) - nJ_n(ak)i,$$

$$k = \sqrt{\varepsilon} k_0,$$

where J_n and Y_n are Bessel function of the first kind and second kind, respectively. The input impedance can be written as following with respect to Equation (27):

$$Z_{in} = -\frac{1}{I_0}\int_0^h E_z(r_0) dz. \quad (28)$$

IV. RESULTS

Figure 3 and Fig. 4 show the comparison between theoretical and CST studio input impedance for two values of substrate permittivity. In order to examine modes behavior in this paper we consider PEC patch and PEC ground plane in conjunction with lossless dielectric.

For each calculation we consider 10 modes, the modes having order of greater than 10 were found to have insignificant effect on the calculated input impedance. It is seen that the mode matching results are close to that obtained by the CST studio simulation except for negligible shift in frequency. Figure 5 shows the effect of source position on input impedance. As it can be seen by increasing the radius of feed position the input impedance increases and the results are close to CST studio results.

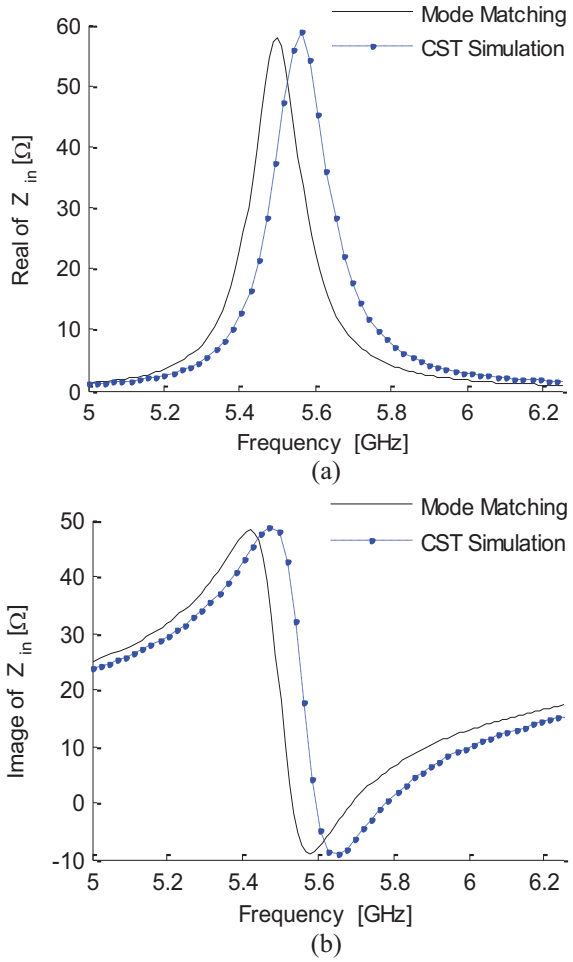

Fig. 3. Comparison between CST studio result and mode matching method. $a = 10mm, h = 1mm, \varepsilon_r = 2.2, r_0 = 2.725mm$, (a) real part and (b) imaginary part, respectively.

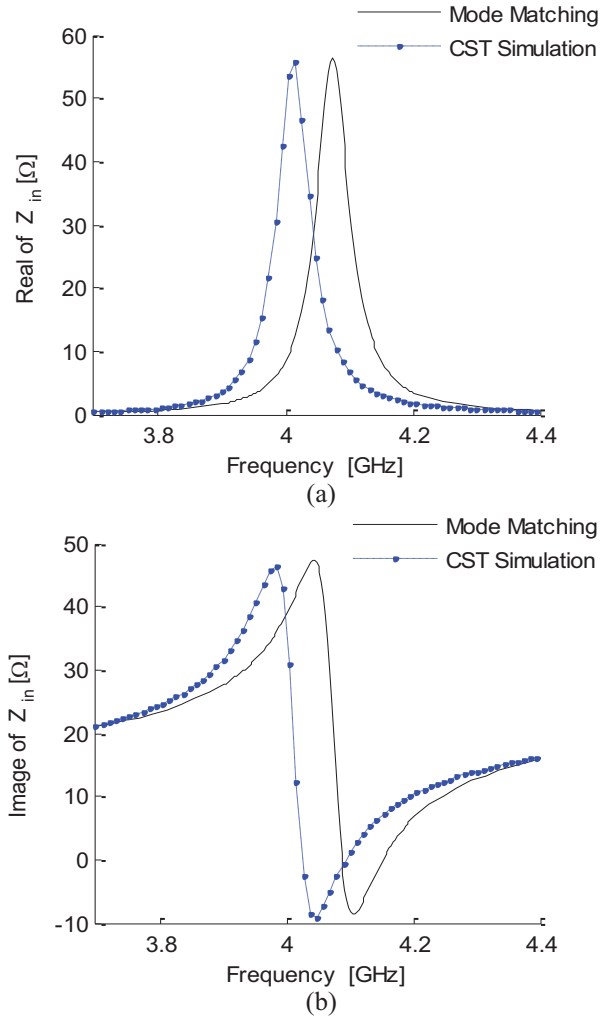

Fig. 4. Comparison between CST studio result and mode matching method. $a = 10mm, h = 1mm, \varepsilon_r = 4.4$, $r_0 = 2.1mm$, (a) real part and (b) imaginary part, respectively.

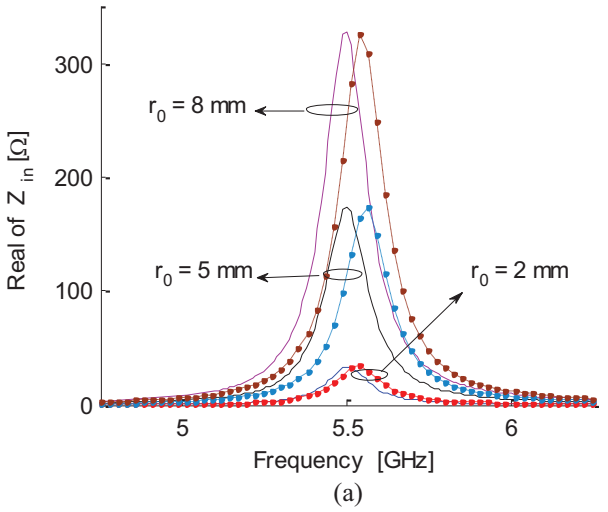

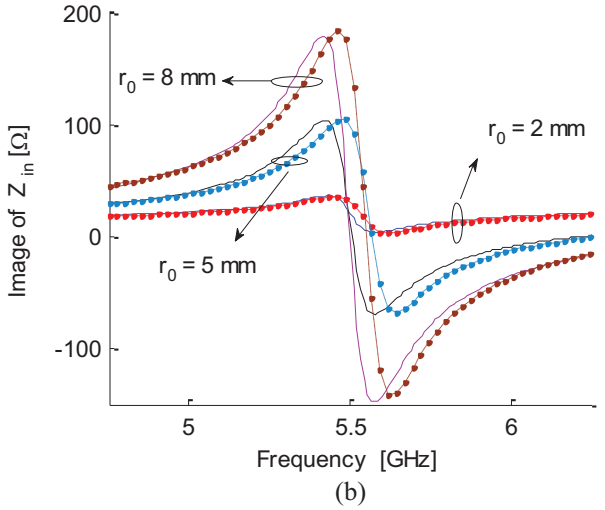

Fig. 5. Effects of source position on input impedance. $a = 10mm, h = 1mm, \varepsilon_r = 2.2$, (a) real part and (b) imaginary part, respectively. Dashed lines: mode matching, dotted lines: CST studio simulation.

IV. CONCLUSION

In this paper, mode matching technique was used to calculate the input impedance of antenna for analysis of microstrip antenna with both electric and magnetic surface current on sidewall in cavity model. The results are in good agreement with simulation results except for about 2% shift in frequency. It is believed that these shifts in frequency in comparison with simulation results are because of fringing field at the edge of the patch and these can be compensated with defining better approximation for effective radius of patch. We believe that the concept that is used in this paper can be extended to other cylindrical shape structure like cylindrical slot.

REFERENCES

[1] T. Samaras, A. Kouloglou, and J. N. Sahalos, "A note on the impedance variation with feed position of a rectangular microstrip-patch antenna," *IEEE Antennas and Propagation Magazine*, vol. 46, no. 2, pp. 90-92, 2004.

[2] T. Günel, "Modified calculation for input impedance of probe-fed and inset-fed rectangular microstrip antennas," *Microwave and Optical Technology Letters*, vol. 57, no. 7, pp. 1650-1652, 2015.

[3] Y. Sazanmi and A. Ishimaru, "A theoretical study of the input impedance of a circular microstrip disk antenna," *IEEE Transactions on Antennas and Propagation*, vol. 29, no. 1, pp. 77-83. 1981.

[4] J. Kong, "Analysis of a circular microstrip disk antenna with a thick dielectric substrate," *Antennas and Propagation, IEEE Transactions on*, vol. 29, no. 1, pp. 68-76, 1981.

[5] K.-F. Lee, K. Y. Ho, and J. S. Dahele, "Circular-disk microstrip antenna with an air gap," *Antennas and Propagation, IEEE Transactions on*, vol. 32, no. 8, pp. 880-884, 1984.

[6] W. F. Richards, Y. T. Lo, and D. D. Harrison, "An improved theory for microstrip antennas and applications," *Antennas and Propagation, IEEE Transactions on*, vol. 29, no. 1, pp. 38-46, 1981.

[7] J. Y. Siddiqui and D. Guha, "Improved formulas for the input impedance of probe-fed circular microstrip antenna," In *Antennas and Propagation Society International Symposium, 2003, IEEE*, vol. 3, pp. 152-155, 2003.

[8] C. S. Gürel, E. Aydın, and E. Yazgan, "Computation and optimization of resonant frequency and input impedance of a coax-fed circular patch microstrip antenna," *Microwave and Optical Technology Letters*, vol. 49, no. 9, pp. 2263-2267, 2007.

[9] G. Kumar and K. P. Ray, *Broadband Microstrip Antennas*, Artech House, 2002.

[10] M. J. Mehler, T. S. M. Maclean, and A. K. Abbas, "Input impedance of a circular microstrip disc antenna using mode matching," *Electronics Letters*, vol. 22, no. 7, pp. 362-363, 1986.

[11] G. Bahl and P. Ramesh, *Microstrip Antenna Design Handbook*, Artech House, 2001.

[12] C. Balanis, *Advanced Engineering Electromagnetics*, John Wiley & Sons, 2012.